Towards the simulation of partially coherent x-ray scattering experiments

Cite as: AIP Conference Proceedings **2054**, 060079 (2019); https://doi.org/10.1063/1.5084710
Published Online: 16 January 2019

Lutz Wiegart, Maksim Rakitin, Yugang Zhang, Andrei Fluerasu, and Oleg Chubar

Towards the Simulation of Partially Coherent X-ray Scattering Experiments

Lutz Wiegart[1, a)], Maksim Rakitin[1], Yugang Zhang[1], Andrei Fluerasu[1] and Oleg Chubar[1]

[1]*National Synchrotron Light Source II, Brookhaven National Laboratory, NY, USA 11973*

[a)]Corresponding author: lwiegart@bnl.gov

Abstract. Exploiting the coherence properties in the hard X-ray regime is an important topic for the emerging ultra-low-emittance synchrotron storage rings. The Coherent Hard X-ray (CHX) beamline at the National Synchrotron Light Source II (NSLS-II) is exploiting the coherent flux to enable best-in-class time-resolved coherent scattering techniques such as X-ray Photon Correlation Spectroscopy (XPCS) or X-ray Speckle Visibility Spectroscopy (XSVS). Based on the commissioning results, a realistic simulation of the whole beamline, including source and optics, has been performed leveraging a 'virtual beamline' module of the 'Synchrotron Radiation Workshop' (SRW) code in a web browser based interface to the code named 'Sirepo'. This virtual beamline capability is used here to simulate partially coherent small angle scattering patterns of samples relevant to the CHX science case, mimicking 'detector images' of real experiments. Such source-to-detector simulations of experiments allow for an accurate estimation of feasibility of a given experiment, for an optimization of the beamline setup and interpretation of experimental results.

1. INTRODUCTION

Development, commissioning, and operations of X-ray sources and instruments at light source facilities such as synchrotrons and free electron lasers, make widely use of the high accuracy physical optics calculation methods available in 'Synchrotron Radiation Workshop' (SRW) [1] [2]. The 'Coherent Hard X-ray' (CHX) scattering beamline at the 'National Synchrotron Light Source II' (NSLS-II) at Brookhaven National Laboratory has employed such calculations to simulate performance of insertion devices and beamline optics during the design phase [3] [4]. With the start of beamline operations in 2014, substantial efforts were made to benchmark the performance of the beamline by comparing measured and simulated key performance parameters, such as spectral photon flux, focal spot sizes, and transverse X-ray beam coherence. Such measurements and simulations revealed, for instance, the impact of monochromator crystals with imperfect surface polishing [5]. They were also used to diagnose and mitigate alignment problems between the electron beam in the storage ring and the magnetic arrays of the insertion device, restoring virtually the theoretical achievable spectral flux for this beamline [6] [7].

Today, the performance of the CHX beamline in terms of source and optics is well understood for the small angle scattering regime and reproducible by simulations. Where deviations from theoretical performance could not be resolved, they are taken into account in the simulations as imperfect beamline elements. Such cases include the insertion device being based on the measured magnetic field and mirror and crystal surfaces including height profile data. The focus is now shifting towards the simulation of experiments and their comparison with 'real' data. The scientific mission of the CHX beamline comprises the investigation of structure-dynamics relations in soft- and hard-condensed matter samples, by techniques such as X-ray Photon Correlation Spectroscopy (XPCS) [8], X-ray Speckle Visibility Spectroscopy [9] or speckle echoes [10]. For many experiments exploiting these techniques, the ability to trade photon flux (determining time resolution) versus transverse degree of X-ray beam coherence (determining speckle visibility) determines the data quality or even feasibility of an experiment. The CHX beamline was designed to easily realize such trade-off by selecting the phase space of the source that is focused down to the sample and used in the experiment. Simulations can greatly help to determine optimal source and optics settings for

Proceedings of the 13th International Conference on Synchrotron Radiation Instrumentation – SRI2018
AIP Conf. Proc. 2054, 060079-1–060079-7; https://doi.org/10.1063/1.5084710
Published by AIP Publishing. 978-0-7354-1782-3/$30.00

a given sample and experiment, select the optimal detector distance and estimate intensity distributions and required acquisition times. The SRW code employed to simulate source and optics performance, as well as scattering pattern of samples at the detector position, uses Fourier optics and compatible methods for fully coherent radiation propagation. Partially coherent radiation propagation is based on adding propagation results for fully coherent propagation emitted by 'macro-electrons' seeded over the electron beam phase space [4]. The fully coherent radiation propagating through a thin sample is simulated by the multiplication of the radiation transverse electric field components by complex transmission functions, which can alter amplitudes and phases of the field components. The propagation of the transmitted electric field from the sample to the detector is simulated by a far-field drift space propagator.

In this paper we describe the layout and performance of the source and optics of the CHX beamline and show that measured and simulated parameters are in good agreement. This is the basis for quantitative simulations of partially coherent sample scattering pattern as 'virtual' data. As an intermediate step, slit diffraction pattern are simulated as detector images and compared to the corresponding measurements. Scattering patterns from a lithographic sample are simulated as detector images and quantitatively compared to the experimental data using the standard analysis code available at the CHX beamline.

2. SOURCE AND BEAMLINE OPTICS

Understanding source and optics performance and achieve agreement between simulations and measurements is a prerequisite for performing quantitative simulations of experimental data. The optical layout of the CHX beamline for a small angle scattering experiment is shown in Fig. 1.

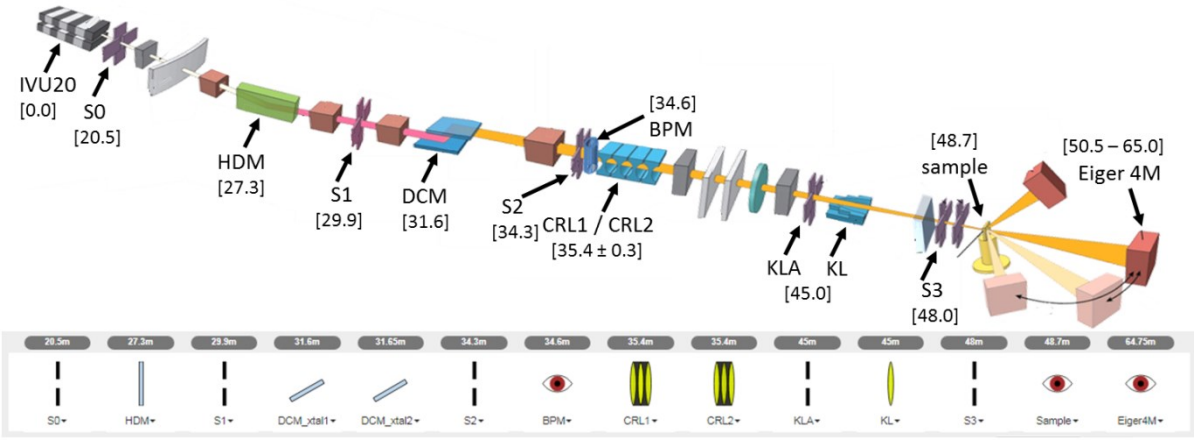

FIGURE 1. Top: schematic layout of the CHX beamline for a small angle scattering experiment. The beamline components include an in-vacuum undulator (IVU20), a Horizontally Deflecting Mirror (HDM), a Double Crystal Monochromator (DCM), Be Compound Refractive Lenses (CRLs), a Si kinoform lens (KL), and a number of slits with square apertures (S0-S3). The numbers in square brackets denote the distance of the components from the center of the storage ring straight section. Bottom: representation of optical layout in the web browser based interface to SRW. Note that the source (IVU20) and electron beam are defined in a separate tab of the web interface.

The X-ray source is an in-vacuum undulator with 20 mm magnetic period (IVU20), located in a low-beta straight section of the NSLS-II storage ring. The X-ray beam is horizontally deflected by a flat mirror and monochromatized by a double crystal monochromator, equipped with Si111 and Si220 crystal sets. Vertical focusing is achieved by combinations of compound refractive lenses (radius of curvature R=0.5 mm and R=1.5 mm) in a transfocator device. Horizontal focusing is achieved by kinoform lenses [10] etched in silicon. For SAXS experiments, the nominal focal position is close to the S3 aperture, from which the beam propagates onto the sample, thereby illuminating the sample with an almost symmetrical spot size of about 10×9 μm^2 (v×h).

The key performance parameters of a coherent scattering beamline include the coherent flux, the transverse and longitudinal coherence of the X-ray beam and the focal spot size used in the experiment. The coherent flux at a given X-ray energy is determined by the beamline source, i.e. the properties of the electron beam in the straight section and the insertion device. Together with other experimental parameters, such as the sample detector distance

or the detector pixel size, these key performance parameters determine an important figure of merit in coherent scattering applications: the visibility of speckles in the collected scattering pattern. Fig. 2 shows examples of benchmarking three such key performance parameters, comparing measurements with SRW simulations. Fig. 2a) shows the photon flux through a 50×50 μm^2 aperture at the position of S2 for the 7th undulator harmonic around 9650 eV. These measurements were performed after completion of the spectral-flux-based alignment procedure of the insertion device [6]. The intensity of the DCM Bragg scan with the Si111 crystal pair was measured using the fluorescence signal from a 600 nm Ti foil in the BPM and four Si pin-diodes (Hamamatsu, S3590-09) connected to a four channel Picoammeter (AH401D, CAENels). The absolute intensity of this measurement was obtained by converting the photo-current of a Si pin-diode in direct illumination mode to photons per second. Conversion of the measured intensity into the photon flux per unit area and 0.1% bandwidth, the units of the corresponding SRW calculations, was performed as described in [10], assuming ideal performance of HDM and DCM. The SRW calculations used a 'tabulated' undulator, based on the magnetic measurements of the CHX IV20 prior to its installation in the storage ring, and archived values from the accelerator database for electron beam parameters at the time of measurement. The agreement between measurement and simulation in terms of intensity is given by $I_{meas.}/I_{sim.}$ = 90.4%, while the values for the width of the undulator harmonic are $FWHM_{sim.}$ = 54.8 eV and $FWHM_{meas}$ = 55.5 eV. It is noteworthy that the simulations and flux calculations assumed ideal optics, thus the observed minimal deviations include the combined effects of electron beam, magnetic field, HDM, DCM and detectors.

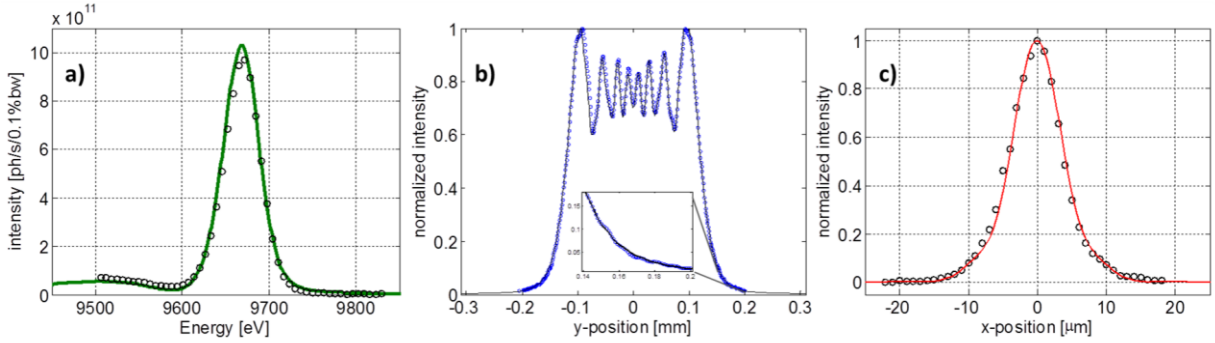

FIGURE 2. a) spectral flux of the 7th undulator harmonic, comparison of measurement (open symbols) and simulation (solid line). b) Measurement (open symbols) and simulation (solid line) of partially coherent diffraction from a 0.2mm vertical aperture of the S2 slit. c) Measurement (open symbols) and simulation (solid line) of the horizontal beam profile at the sample position, resulting from the focusing with a Si kinoform lens.

Fig. 2 b) compares measured and simulated vertical slit scattering profiles at 9.65 keV from the S2 aperture, measured at the sample position. Such slit scattering is a sensitive measure of the transverse X-ray beam coherence. Measurements were performed using a 1 μm aperture in front of a CCD camera with optically coupled fluorescent screen. Simulations employed optics descriptions as realistically as possible, including HDM and DCM height profiles [5], ID magnetic field map and archived electron beam parameters from the time of measurement. Simulation and measurement show excellent agreement and similar comparisons were performed for S2 aperture sizes in horizontal and vertical directions and the sensitivity to source parameters was demonstrated [10]. The longitudinal X-ray beam coherence, defined by the monochromaticity of the X-ray beam, is not a concern in the small angle scattering regime (very short path length differences) and was thus not characterized. Fig. 2 c) displays the horizontal beam profile at the sample position for a typical small angle scattering experiment at 9.65 keV at CHX. The horizontal aperture of the S2 slit was 100 μm and the beam was focused by a silicon kinoform lens to achieve a waist at a longitudinal position close the S3 aperture. The beam profile was measured with a Ni coated Si 'knife edge' and an energy dispersive detector integrating over the Ni fluorescence energies. The model independent FWHMs are 8.5 μm for the measurement and 8.3 μm for the simulation. Similar measurements and simulations were performed for the vertical beam profile as well as for different aperture sizes of S2, relevant to coherent scattering experiments at CHX.

3. COMPARISON OF MEASURED AND SIMULATED SCATTERING PATTERN

Overall, the extensive measurements and simulations performed for key performance parameters of the CHX beamline are in very good quantitative agreement. This stems partly from the beamline source and optics achieving close to as-designed performance, and partly from extensive efforts to include known imperfections in the simulations. As a result, the simulations are capable of quantitatively describing the X-ray beam properties all the way to the sample position, which is the starting point for quantitative simulations of experiments and their comparison with the corresponding experimental data.

3.1 Detector Images of Slit Diffraction

As an intermediate step, partially coherent diffraction images of the square aperture of the S2 slit were collected with the CHX SAXS detector (Eiger X 4M, Dectris, 75 × 75 μm^2 pixel size). Similar images of 'pinhole diffraction' were previously recorded from the KL aperture, using a CCD camera with optically coupled fluorescent crystal (pixel resolution ~0.8 μm) at the sample position [10]. However, due to the limited sensitivity, detector noise, and dynamic range, the weak side-maxima in the interference pattern were only visible close to the center of the diffraction pattern. The Eiger detector, located inside a vacuum chamber connected to an evacuated flight pass, provides in contrast noise-free single photon counting capability at a virtually infinite dynamic range. To compensate for the much larger pixel size of the Eiger detector, an aperture-detector distance of about 31 m was chosen. Nevertheless, the diffraction patterns are under-sampled, i.e. the visibility of fringes is reduced by the detector pixel size. To enable a quantitative comparison, the corresponding simulation datasets were binned to a spatial resolution of 75 × 75 μm^2, mimicking the resolution of the Eiger detector.

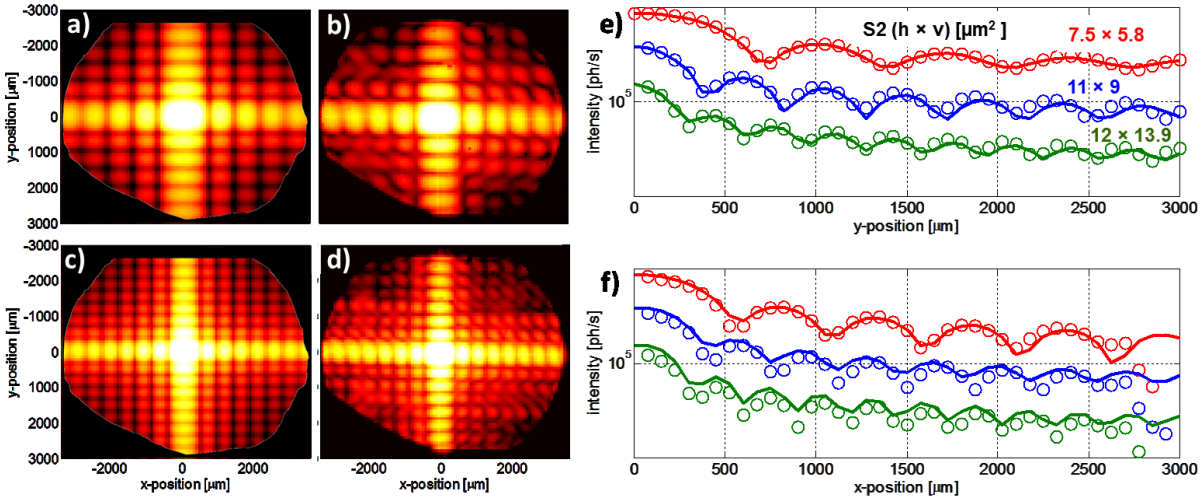

FIGURE 3. Simulated (a) and c)) and measured (b) and d)) partially coherent diffraction pattern from S2, measured at a distance of ~ 31 m downstream with an Eiger X 4M detector at an X-ray energy of 9.65 keV. a) and b): aperture size 7.5 × 5.8 μm^2 (h ×v), c) and d): aperture size 11 × 9 μm^2 (h ×v). Vertical (e)) and horizontal (f)) cuts through partially coherent diffraction pattern for aperture sizes as indicated in the top panel. Open symbols: measured data, solid lines: simulation.

Fig. 3 a) - d) shows simulated and measured partially coherent diffraction pattern for two different sizes of the S2 aperture. The somewhat circular 'mask' limiting the extend of the diffraction pattern stems from the aperture of X-ray windows around the sample position. A similar –artificial- 'mask' was applied to the simulated diffraction pattern for the ease of visual comparability. The measured data shows some distortions, both in terms of intensity and shape of the interference maxima. A likely cause for these distortions are the X-ray windows (~20 μm thick Mica) around the sample position. While in a typical experiment their illuminated area only extends over a few tens to hundreds of micrometers, in this particular configuration they are completely illuminated, including bad regions that would otherwise not be used in experiments. In particular, distortions appear to be largest towards the edge of the aperture, where the deformation of the windows due to the vacuum force is largest. Fig. 3 also shows horizontal and vertical line cuts through the simulated and measured diffraction pattern. The cuts were taken through the center

spot of the 2D diffraction pattern and correspond to one row or column of 75 μm wide detector pixels. The visibility of the fringes in simulation and measurement is comparable, validating the applied 're-sampling' of the propagated wavefront to the detector pixel size.

3.2 Simulation and Measurement of Sample Scattering Pattern

A 'thin', i.e. weakly absorbing, sample can be included in SRW simulations as a transmission type optical element [3] [13]. This transmission object modifies the amplitude and phase of the impinging radiation electric field over the range of horizontal and vertical positions covered by the transmission object and the incoming wavefront. Here the sample was an array of randomly oriented and arranged Au nano-objects of rectangular shape (with ~65 × 58 nm average transverse dimensions and ~50 nm thickness), prepared by lithographic methods at the Center for Functional Nanomaterials (CFN) at BNL. Electron microscopy images and a dedicated module in the Python version of SRW were used to convert the lithographic sample into a transmission object for SRW simulations. The measurements were performed using a standard configuration of the CHX beamline for a coherent small angle scattering experiment: X-rays of energy 9.65 keV were focused in vertical (by means of CRLs) and horizontal (by means of a Si kinoform lens) directions at the position of the S3 slits and propagated onto the sample. Partially coherent scattering patterns were collected with an Eiger X 4M detector at a sample-detector distance of ~16.3 m. Top level beamline control and data acquisition at the CHX beamline use Python-based 'Bluesky' [11], which includes a hardware abstraction layer in Python and a package for databases, used to store experimental and meta-data. For data access and analysis, CHX uses IPython notebooks in Jupyter, were packages for data analysis, e.g for XPCS and XSVS, have been developed.

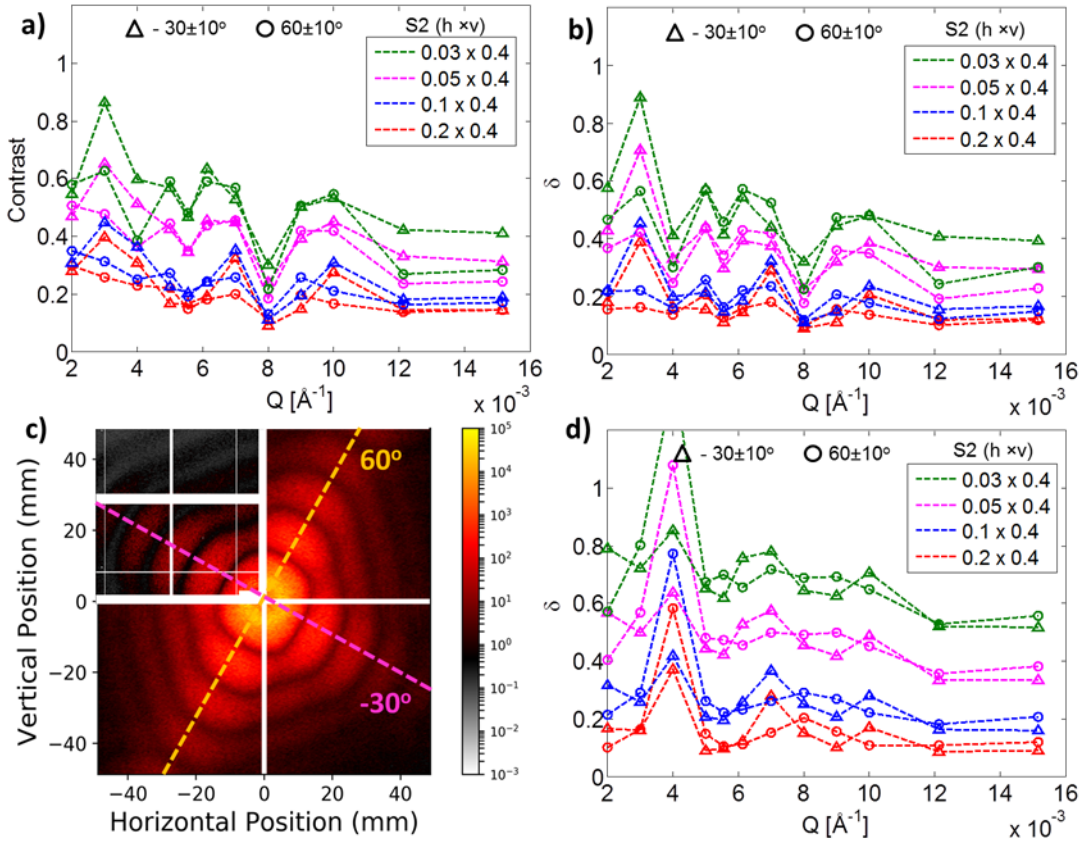

FIGURE 4. Analysis of speckle visibility in simulated and measured partially coherent scattering pattern for different horizontal aperture sizes of S2. a) Contrast parameter from speckle visibility analysis for the measured datasets. b) Standard deviations from the analysis of the measured dataset. c) Simulated partially coherent scattering pattern for S2 = 0.2×0.4 mm^2, upper left quadrant: corresponding measured scattering pattern (white lines correspond to detector module and chip gaps, beamstop, etc.). The directions of -30^o and 60^o, along which the speckle visibility was analyzed, are indicated by dashed lines. d) Standard deviations from the analysis of the simulated datasets.

In order to unify access, analysis, and comparison of both simulated and measured data, a file writer for SRW has been created in 'Bluesky'. This file writer is mimicking a 'detector' that writes simulation data to the database in the same fashion as 'real' detectors at the beamline do. Fig. 4 shows a comprehensive comparison of the speckle visibility from the measured and simulated scattering pattern, for different horizontal aperture sizes of the S2 slit. The horizontal size of S2 is typically used to increase or decrease the degree of transverse coherence of the beam, at the expense of photon flux. While the source is rather coherent in the vertical direction, the amount of horizontal X-ray beam phase space used for the experiment has a strong influence on the degree of coherence and the visibility of speckles in the recorded scattering pattern. Measured and simulated scattering patterns are shown in Fig. 4c) for a horizontal aperture size of 0.2 mm. The visibility was analyzed along two azimuthal directions (indicated as -30^o and 60^o), corresponding to the high intensity features in the scattering pattern. The regions of interest (ROIs) used in the analysis span wavevector transfers Q from 0.002 to 0.01516 $Å^{-1}$, with a Q-width of 5×10^{-4} $Å^{-1}$ and an angular width of $\pm10^o$ around the -30^o and 60^o directions. Fig. 4 a) displays the contrast factor obtained by the speckle visibility analysis described in [9]. The contrast is inverse proportional to the number of coherent modes used in the experiment. As expected, the contrast is increasing as the aperture size is reduced. This speckle visibility analysis is based on photon counting statistics. As the SRW wavefront propagation simulations do not directly produce photon counts, the simulated scattering patterns were analyzed over the same ROIs by calculating the standard deviation δ of the partially coherent scattered intensity from the corresponding incoherent scattered intensity [13]. The incoherent scattering was obtained by smoothing out the speckles using a Savitzky–Golay filter. The results for the different apertures sizes as a function of Q and azimuthal direction are displayed in Fig. 4 d). The same analysis was applied to the measured datasets and the results are shown in Fig. 4 b). For the measured datasets, both the speckle visibility analysis and the standard deviation produce comparable results, thus validating this approach for the quantitative analysis of the simulated datasets. The standard deviation of the simulated scattering pattern shows the same scaling of increasing visibility with decreasing aperture size, however, with some quantitative differences for aperture sizes < 0.1 mm. Interestingly, the difference between measured datasets for S2 horizontal gaps of 0.1 and 0.2 mm is rather small –both in the speckle visibility and the standard deviation analysis – a behavior that is quantitatively reproduced in the analysis of the simulated data.

4. SUMMARY

The advent of ultra-low-emittance synchrotron storage rings provides exciting possibilities for exploiting coherence properties in the hard X-ray regime. The techniques making use of the X-ray transverse coherence include Coherent Diffraction Imaging (CDI) in both Bragg and forward scattering geometries and time resolved coherent scattering such as XPCS or XSVS. A realistic simulation of the CHX beamline at NSLS-II has been implemented in the SRW code, allowing for an accurate and quantitative simulation of key performance parameters. Based on this work, initial tests show that it is now feasible to move towards the quantitative simulations of experimental data, as collected by the beamline detectors. An effort is ongoing to unify the collection, access, and analysis of both simulated and measured data, which will enable the more wide-spread use of studies employing both simulation and measurements.

ACKNOWLEDGMENTS

We would like to thank A. Stein, C. Black, K. Yager and B. Ocko for preparation of samples at CFN/BNL, and D. L. Bruhwiler, R. Nagler, P. Moeler (RadiaSoft) for collaboration on Sirepo and SRW development. The experiment simulation work was supported by US DOE contract DE-SC0012704 and SBIR grant DE-SC0011237.

REFERENCES

[1] O. Chubar and P. Elleaume, in *Proc. EPAC-98*, 1998.

[2] O. Chubar, M. Rakitin, Y. Chen-Wiegart, Y. S. Chu, A. Fluerasu, D. Hidas and L. Wiegart, "Main functions, recent updates, and applications of Synchrotron Radiation Workshop code," in *Proc. of SPIE*, 2017.

[3] O. Chubar, A. Fluerasu, L. Berman, K. Kaznatcheev and L. Wiegart, "Wavefront propagation simulations for beamlines and experiments with "Synchrotron Radiation Workshop"," in *Journal of Physics Conference Series*,

Lyon, FRANC, 2013.

[4] O. Chubar, L. Berman, Y. Chu, A. Fluerasu, S. Hulbert, M. Idir, K. Kaznatcheev, D. Shapiro, Q. Shen and J. Baltser, "Development of partially-coherent wavefront propagation simulation methods for 3rd and 4th generation synchrotron radiation sources," in *Proc. of SPIE*, 2011.

[5] L. Wiegart, A. Fluerasu, D. Bruhwiler and O. Chubar, "Partially Coherent Wavefront Propagation Simulations: Mirror and Monochromator Crystal Quality Assessment," in Proceedings of SRI 2015, *AIP Conference Proceedings*, New York, NY, 2016.

[6] O. Chubar, C. Kitegi, Y. K. Chen-Wiegart, D. Hidas, Y. Hidaka, T. Tanabe, G. Williams, J. Thieme, T. Caswell, M. Rakitin, L. Wiegart, A. Fluerasu, L. Yang, S. Chondanakar and M. Zhernenkov, "Spectrum-Based Alignment of In-Vacuum Undulators in a Low-Emittance Storage Ring," *Synchrotron Radiation News,* vol. 31, no. 3, pp. 4-8, 2018.

[7] O. Chubar, Y. Chu, X. Huang, S. Kalbfleisch, H. Yan, T. Shaftan, G. Wang, Y. Cai, A. Suvorov, A. Fluerasu, L. Wiegart, Y. Chen-Wiegart, J. Thieme, G. Williams, M. Idir, T. Tanabe, P. Zschack and Q. Shen, "Initial Performances of First Undulator-Based Hard X-Ray Beamlines of NSLS-II Compared to Simulations," in *Proceesings of SRI 2015*, *AIP Conference Proceedings,* New York, NY, 2016.

[8] O. G. Sphyrko, "X-ray photon correlation spectroscopy," *Journal of Synchrotron Radiation,* vol. 21, p. 1057–1064, 2014.

[9] L. Li, P. Kwasniewski,, D. Orsi, L. Wiegart, L. Cristofolini, C. Caronna and A. Fluerasu, "Photon statistics and speckle visibility spectroscopy with partially coherent X-rays," *Journal of Synchrotron Radiation,* vol. 21, pp. 1288-1295, 20014.

[10] M. C. Rogers, K. Chen, L. Andrzejewski, S. Narayanan, S. Ramakrishnan, R. L. Leheny and J. L. Harden, "Echoes in x-ray speckles track nanometer-scale plastic events in colloidal gels under shear," *Phys. Rev. E,* vol. 90, p. 062310, 2014.

[11] K. Evans-Lutterodt, J. Ablett, A. Stein, C. Kao, D. Tennant, F. Klemens, A. Taylor, C. Jacobsen, P. Gammel, H. Huggins, S. Ustin, G. Bogart and L. Ocola, "Single-element elliptical hard x-ray micro-optics," *Optics Express,* vol. 11, no. 8, pp. 919-926, 2004.

[12] L. Wiegart, M. Rakitin, A. Fluerasu and O. Chubar, "X-ray optical simulations supporting advanced commissioning of the coherent hard X-ray beamline at NSLS-II," in *Proc. of SPIE*, 2017.

[13] O. Chubar, M. Rakitin, Y. K. Chen-Wiegart, A. Fluerasu and L. Wiegart, "Simulation of experiments with partially coherent x-rays using Synchrotron Radiation Workshop," *Proc. of SPIE,* vol. 10388, p. 1038811, 2017.

[14] A. Arkilic, D. B. Allan, T. Caswell, K. Lauer and S. Abeykoon, "Towards Integrated Facility-Wide Data Acquisition and Analysis at NSLS-II," *Synchrotron Radiation News,* pp. 44-45, 2017.